Multiscale Model for Photoinduced Molecular Motion in Azo Polymers

Mathieu L. Juan,[†] Jérôme Plain,[†,*] Renaud Bachelot,[†] Pascal Royer,[†] Stephen K. Gray,[‡] and Gary P. Wiederrecht[‡]

[†]Laboratoire de Nanotechnologie et d'Instrumentation Optique, ICD CNRS FRE 2848, Université de technologie de Troyes, BP 2060, 10000 Troyes, France, and [‡]Center for Nanoscale Materials, Argonne National Laboratory, Argonne, Illinois 60439

ABSTRACT Light-induced isomerization processes in azobenzene-containing polymers produce mass transport that is of much interest for nanoscale imaging and lithography. Yet, despite the development of numerous models to simulate the mass transport mechanism, no model precisely describes all the experimental observations. We develop a new statistical approach that correctly reproduces light-driven mass motion in azobenzene-containing polymers with a high degree of accuracy. Comparisons with experiments show that our model predicts the nanoscale topographic modifications for many different incident field configurations, including optical near-fields produced by plasmonic structures with complex polarization states. In particular, the model allows the detailed molecular motions that lead to these topographic modifications to be identified.

KEYWORDS: photoisomerizable azo polymers · nanolithography · molecular motion modeling · mass transport · photochemical imaging · plasmonics

The observation of mass transport in photoisomerizable azo polymers has generated considerable interest as a fundamental light-matter interaction problem.[1,2] Furthermore, the dramatic topography changes induced by the light-induced mass transport may have applications to micro- and nanoscale imaging and lithography. For example, azobenzene-containing polymers undergo a trans-to-cis light-induced isomerization and transport process that has recently been exploited to image the confined fields at the focus plane of a high numerical aperture objective lens[3] and to image the evanescent fields produced by nanoscale plasmonic structures under illumination.[4] As shown by Hubert *et al.*,[4] the topography produced in the polymer film allowed for the direct visualization of the near-field plasmonic dipole in the metallic nanostructures for the first time without using optical scanning probe techniques. The spatial resolution of the topographic imaging was shown to be approximately 20 nm. This experiment exemplifies that, in order to understand and utilize mass transport in photoisomerizable azo polymers, a model that fundamentally and reliably explains the light-matter interaction mechanism is needed. A correct model must work under a wide range of potential illumination conditions, including propagating or evanescent fields, wide or narrow wavevector ranges, anisotropic polarization distributions, *etc.*

While several models have been proposed (a good review on the models describing the SRG formation is given by Lagugné Labarthet *et al.*[5]), none are always successful under this range of illumination conditions. We first note the primary set of existing models. Barrett *et al.*[6] proposed a model involving a pressure gradient deformation induced by the free space changes between the different geometries of trans and cis isomers. Due to the cis isomer's higher free space requirement, viscoelastic flow is generated in the bright regions, according to Navier−Stokes viscosity equations. This photoinduced viscosity flow agrees well with surface relief grating (SRG) experiments.[7] Yet, the polarization sensitivity is not well-reproduced, suggesting the necessity to take into account the azobenzene dipole.[8] Pedersen *et al.*[9] developed a mean field model based on the interaction between molecular dipoles. The photoinduced alignment of the molecule produced polymer flow toward the bright regions due to dipolar attraction between the aligned molecules. Although the results are consistent with microcrystallization experiments, the model contradicts observations for amorphous polymers. Recently, Barada *et al.*[10,11] proposed a model based on the semi-implicit moving-particle method. The azobenzene-containing polymer is regarded as a viscous fluid, and the

*Address correspondence to jerome.plain@utt.fr.

Received for review March 17, 2009 and accepted May 05, 2009.

Published online May 13, 2009.
10.1021/nn900262e CCC: $40.75

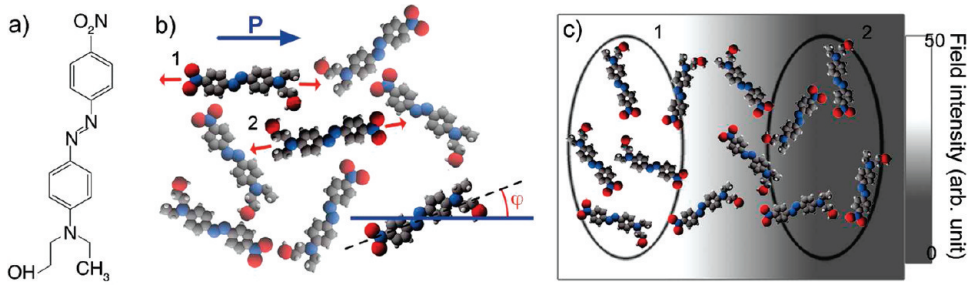

Figure 1. (a) Chemical structure of the azobenzene Disperse Red 1. (b) Schematic view of the azobenzene vectorial sensitivity. In the idealized 2D case with a linearly polarized incident field, molecules with the higher absorption probability are the ones oriented along the polarization. (c) Within a field gradient, the molecules most likely to absorb are the ones in the high intensity region (zone 1 in c)

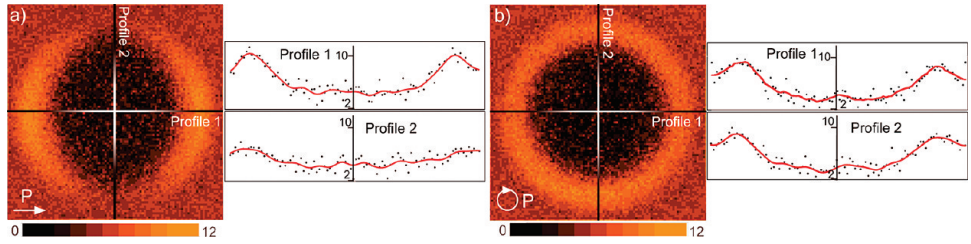

Figure 2. Calculated topographies for the Gaussian beam with different polarizations to emphasize the polarization sensitivity. The linearly polarized Gaussian beam (a) gives rise to a strongly asymmetric topography, while the circularly polarized beam (b) produces a symmetric pattern. Excellent agreement with the experimental results published by Bian *et al.* is found.[16]

molecular motion is related to an optical force gradient and volume change between trans and cis isomers. This model gives good results for the SRG generation and erasure. Later work also reported good agreement with the near-field-induced modification obtained through a simple nanoaperture.[12] However, it does not account for molecular orientation, so that the photoinduced reorientation is not reproduced. Lefin *et al.*[13] developed an anisotropic diffusion model wherein the photoisomerization cycles translate the azobenzene molecules along their long axis. This inchworm translation model gives a physically appealing interpretation of the migration mechanism. Yet, in this model, the orientational distribution of the azobenzene is a parameter, so that the orientational hole burning observed during SRG formation cannot thus be reproduced.[14] More recently, a random-walk model was presented by Bellini *et al.*[15] While hypotheses and phenomenology were discussed in some details, no actual simulations of topographies under complex illuminations were presented. Furthermore, one effect of great interest—the polarization sensitivity of the mass transport—constitutes a hypothesis, while in our model, this effect is a consequence.

In this article, we report a statistical model based on fundamental molecular dipole−light interactions that reproduces the experimental results under widely varying conditions and yields a better understanding of the light-induced mass transport process. We emphasize multiscale aspects of the model, addressing large-scale mass transport and single-molecule motion mechanisms. Moreover, we show the potentiality of our model to predict the topography induced by complex plasmonic nanostrutures as coupled nanoantennaes. This has significant ramifications for the optical control of molecular motion in soft materials.

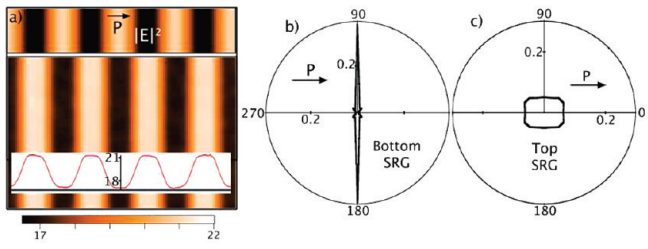

Figure 3. SRG formation under P-type configuration; the incident intensity is shown in the top part of (a). The simulated topography in the bottom of (a) reveals a well-defined SRG. Along with the topography, molecular orientations were retrieved in (b) for the high intensity regions (bottom SRG) and (c) for the low intensity regions (top SRG) revealing strong photo-orientation.

RESULTS AND DISCUSSION

Our model ("photoinduced molecular diffusion model" or PIMD model) is a statistical model relying on a 3D Monte Carlo approach to describe photoinduced molecular motion within the polymer system. The photoactive azobenzene dye molecule is represented in Figure 1a. In the experiments, such dye molecules are grafted to linear chains of PMMA (not shown here).[3,4]

We work at a constant temperature that is near or below the glass transition temperature (T_g) to allow molecular displacement and to limit temperature-induced Brownian motion. The PIMD model is then based on three fundamental hypotheses concerning the displacement of the azobenzene molecules:

(i) Each dye molecule must absorb a photon to undergo an isomerization. The absorption probability is given by $P_{abs} \propto |\mu \times E|^2 \propto |E|^2 \cos^2 \varphi$, with φ being the angle between the direction of the local incident field, E, and the molecular dipole, μ.

(ii) The movement of a dye molecule occurs along the axis of the molecule (identified as the direction of the molecular dipole) as described by the inchworm

translation model proposed by Lefin *et al.*[13] L is the average translation length.

(iii) A dye molecule moves from a hole in the polymer matrix to another hole. From a material point of view, the hole concept corresponds to an area with free space available in the polymer matrix. Then, this free space induces a lower local density compared to the maximum density of the polymer film. From a mathematical point of view, the hole concept is defined between two limiting values of the local density of the polymer film. If the local density is higher (lower) than a certain value d_{high} (d_{low}), the translation process is impossible. We assume that the probability distribution is defined by a Lorentzian function of the local density. Then, a molecule is only allowed to move to a new position according to a joint probability $P_{A\rightarrow B} = P_A \times P_B$ formed from a probability for it to leave its current position P_A, and one for it to occupy the new position P_B.

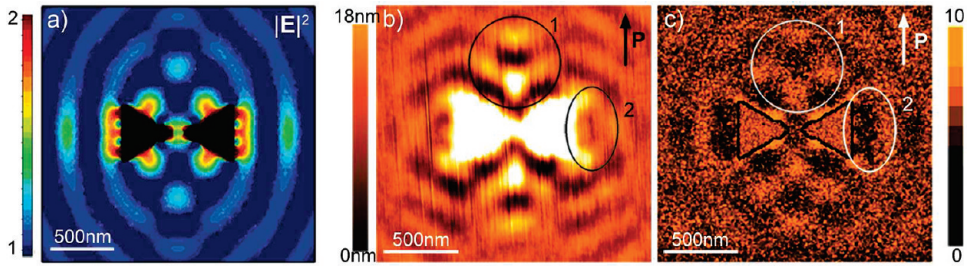

Figure 4. The "bow-tie" structure consists of two silver triangles produced by electron beam lithography on a glass substrate. The calculated electric field for this structure is presented in (a). (b) Experimental and (c) simulated topography.

Several additional hypotheses are required to account for the nature of the polymer matrix and the forces experienced by the azobenzene molecules:

(iv) Short-range interactions (*e.g.*, van der Waals interactions) are accounted for with a random reorientation of the nearest neighbors in the direction of the moving molecule.

(v) Long-range interactions of azobenzene molecules on the same chain are accounted for as follows. Each time an azobenzene group moves, a random set of n molecules grafted in the same polymer chain, within a sphere of radius R, is selected. These molecules are then randomly reoriented in the direction of the moving molecule. The grafting density is correlated with n, and free polymer chain length (correlated with the molecular weight or the cross-linking density) and radius of gyration are correlated with R. Note that, to really take into account the cross-linking density, an additional condition must be applied to the considered molecule which will not be allowed to quit the sphere of radius R.

Figure 1b illustrates hypothesis (i) in the simplified case of a linearly polarized uniform electromagnetic field. Molecules oriented along the polarization direction (*e.g.*, molecules 1 and 2) are more likely to absorb a photon and thus to undergo a trans−cis−trans isomerization cycle. Considering the same system, but with a field intensity gradient (Figure 1c), the absorption probability for molecules in the high intensity area (circled zone 1) will be higher than for molecules in the low intensity area (circled zone 2). For a 3D idealized case with $\boldsymbol{E_1} = E_1\mathbf{e_x}$ and $\boldsymbol{E_2} = E_2\mathbf{e_x}$ (with $\mathbf{e_x}$ a normalized vector along the polarization direction), the local electric fields in specific parts of zones 1 and 2, respectively, the absorption probability is given by

$$P^k_{abs}(\theta,\phi) = C|E_k|^2\cos^2\theta\sin^2\phi \quad k = 1,2 \qquad (1)$$

where C is a constant, and (θ,ϕ) define the orientation of the molecule in spherical coordinates. Considering an isotropic distribution of molecular orientations $\rho(\theta,\phi)$, the molecular flux from zone 1 to zone 2 along the polarization direction $\mathbf{e_x}$ is given by

$$F_{1\rightarrow 2} = \int_{-\pi/2}^{\pi/2}\int_0^{\pi} l(\theta,\phi)\rho(\theta,\phi)P^1_{abs}(\theta,\phi)\sin\theta\, d\theta\, d\phi \qquad (2)$$

where $l(\theta,\phi) = L\cos\phi\sin\theta$ is the photoinduced displacement along $\mathbf{e_x}$.

$$F_{2\rightarrow 1} = \int_{\pi/2}^{3\pi/2}\int_0^{\pi} l(\theta,\phi)\rho(\theta,\phi)P^2_{abs}(\theta,\phi)\sin\theta\, d\theta\, d\phi \qquad (3)$$

$$F_{1\rightarrow 2} + F_{2\rightarrow 1} = CL(|E_1|^2 - |E_2|^2)\int_{-\pi/2}^{\pi/2}\int_0^{\pi}\rho(\theta,\phi)\cos^3\theta\sin^3\phi\sin\theta\, d\theta\, d\phi \qquad (4)$$

We assume that the molecule displacement occurs along the vector parallel to the dipole axis. This hypothesis implies that the displacement only occurs in the forward direction (NO_2 group, Figure 1a). Considering forward ($l(\theta,\phi)$) and backward ($-l(\theta,\phi)$) motion equally probable, the expression of the flux will be

$$F^*_{1\rightarrow 2} = \frac{1}{2}\int_{-\pi/2}^{\pi/2}\int_0^{\pi} l(\theta,\phi)\rho(\theta,\phi)P^1_{abs}(\theta,\phi)\sin\theta\, d\theta\, d\phi + \frac{1}{2}\int_{\pi/2}^{3\pi/2}\int_0^{\pi}(-l(\theta,\phi))\rho(\theta,\phi)P^1_{abs}(\theta,\phi)\sin\theta\, d\theta\, d\phi \qquad (5)$$

It clearly appears from eq 5 that the equiprobable forward−backward displacement does not change the migration mechanism ($F^*_{1\rightarrow 2} = F_{1\rightarrow 2}$). These simplified analytical expressions underline the macroscopic tendency of the azobenzene-containing polymer films to accumulate in the lower intensity regions. Indeed, when $|E_1|^2 > |E_2|^2$, the resulting molecular flux ($F_{1\rightarrow 2} + F_{2\rightarrow 1}$) proceeds from zone 1 to zone 2 in Figure 1c.

Our first examples are designed to reproduce the far-field optical experiments obtained with Gaussian beams,[16] or holographic patterns.[17,18] To emphasize the

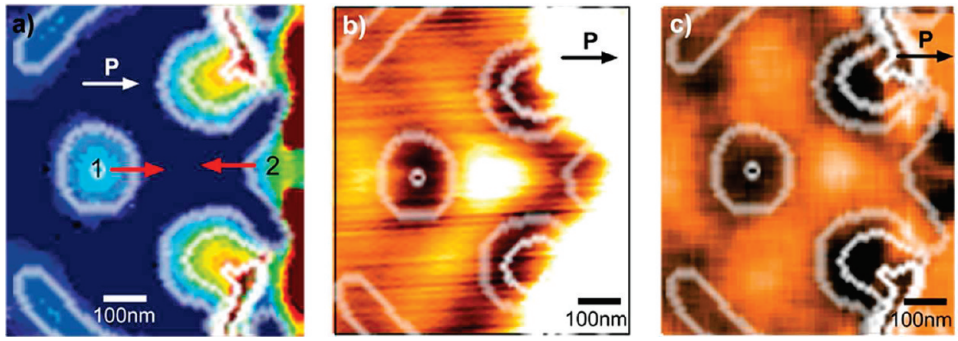

Figure 5. Optical trapping induced by two mass migrations leading to the formation of one localized matter accumulation. (a) Iso-contours of the electric field intensity where 1 and 2 are the high intensity regions inducing the mass migration (red arrows) leading to the formation of a topography maximum. Experimental and simulated topographies are shown in (b) and (c), respectively. Electric field iso-contours are also superimposed to indicate the high intensity regions.

effect of the polarization, different polarization configurations are explored. Panels a and b in Figure 2 show the calculated topographies for the Gaussian beams, polarized linearly and circularly, respectively. For the case of linear polarization, the mass transport is mainly along the polarization direction. This configuration induces a strong topographic asymmetry, particularly when compared with the topography obtained with the circularly polarized configuration, in agreement with experimental results.[16] Topographic profiles are shown next to the images to underscore the polarization sensitivity of this system.

We present only P-polarization results for SRG because we have completed and published elsewhere a more complete study of SRG formation.[19] The simulated topography (Figure 3a) has been smoothed using a simple running average method. The model reproduces the SRG obtained with P-type configurations, the peak being formed in the low intensity regions. In addition to the topography, we were able to obtain the molecular orientation at different positions in the SRG. The orientation distributions presented by polar diagrams in Figure 3b,c have been normalized. In the bottom SRG regions (Figure 3b), corresponding to the high intensity region of the incident field, the molecules show a very strong photoinduced alignment perpendicular to the incident field. This orientational hole burning has been extensively explained and used in many applications.[5,20−22] Conversely, at the top SRG regions, the distribution remains almost isotropic because the incident field intensity is low (the square shape is induced by the discretization of molecular orientation). These results provide interesting perspectives for birefringence studies in azobenzene polymer films obtained with complex incident fields.

We now consider the more complex polymer migration features that result from the wide range of wavevectors and polarization anisotropies within the optical near-field range of metallic nanostructures. On the basis of recent work, we simulate the topographic modifications induced by the optical near-field of a silver "bow-tie" structure.[23] The experimental setup consists of a lithographic bow-tie formed with two facing 400 nm silver triangles. The sample is coated with an azobenzene polymer layer. The complete discussion of the setup and the topographic modifications can be found in the recent publication of Hubert *et al.*[23] The electromagnetic vectorial field used to simulate the topography has been calculated using a discrete dipole approximation 5 nm above the particle. Figure 4a shows the calculated field intensity in the vicinity of the bow-tie illuminated at the wavelength $\lambda = 514$ nm, with a linear polarization perpendicular to the long bow-tie axis. The experimentally obtained topography with an atomic force microscope (AFM) is presented in Figure 4b. Using the computed electromagnetic field, we obtain the simulated topography shown in Figure 4c. Please note that Figure 4a,b has been previously published[23] but is presented to show that this model reproduces major topographic structures well. Indeed, the features referred to as optical trapping in the publication of Hubert *et al.* are clearly simulated. See, for example, the features within circle 1 in Figure 4b and the corresponding simulation result, Figure 4c, which clearly exhibits them. Another complex structure is highlighted on the side of the triangles (circle 2).[23]

To underline the mechanism leading to such features, an iso-contour mask is produced using the field intensity map (Figure 5a) and reproduced on the experimental topography (Figure 5b) and the simulated topographies (Figure 5c). The positions of the high intensity re-

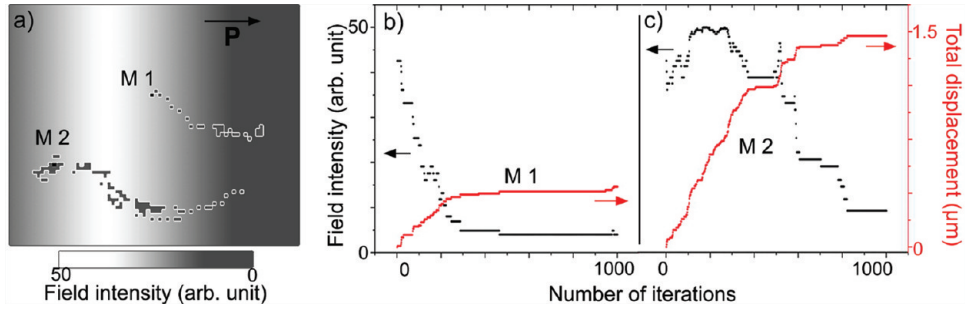

Figure 6. Tracking of individual molecules exposed to a linearly polarized field gradient: (a) two molecules (M1 and M2) have been tracked. The total displacement of the molecules, along with the local field intensity for each occupied position, is shown in (b) and (c) for M1 and M2, respectively.

gions 1 and 2 in Figure 5a induce two contributing mass migrations leading to the formation of a strong topographic maximum. This maximum of topography is believed to correspond to a minimum of the electromagnetic near-field resulting from the destructive interference at a specific place between many evanescent wavelets emitted by the whole structure. On the other hand, this minimum is surrounded by electromagnetic hot spots created by strong constructive interferences. This maximum of topography is clearly visible in the experimental image and is accurately reproduced by the model. The simulated topography has been smoothed using a centered running average method.

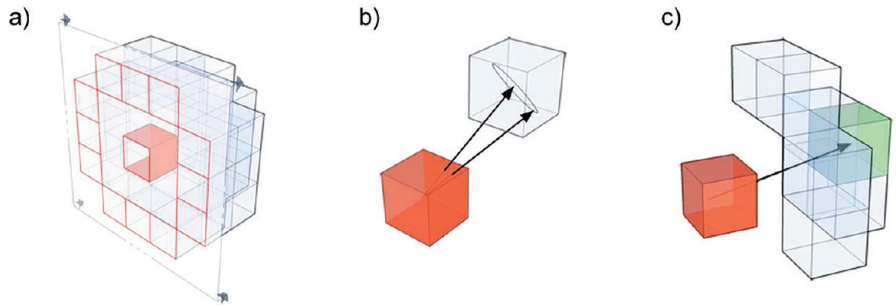

Figure 7. Schematic representation of (a) a cut of the 54 orientational discretizations. The central red box represents the molecule position, while the surrounding boxes define the orientation vector. (b) Within each box, a small random variation of the molecule orientation is taken to reduce discretization impact over the evaluation of the absorption probability. (c) Accessible reorientation vectors are defined to be the adjacent boxes to the actual orientation of the molecule (green box).

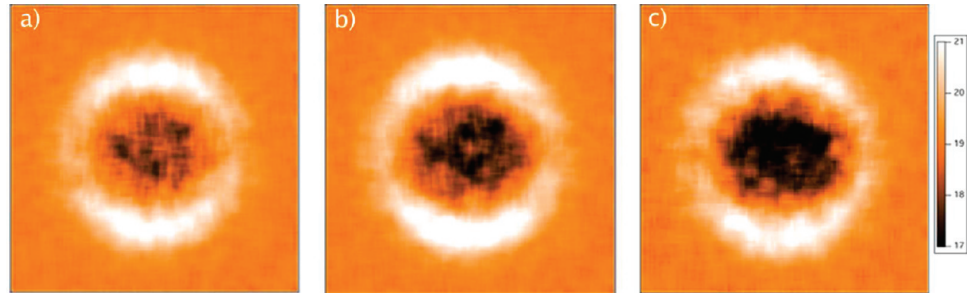

Figure 8. Effect of the translational mean path on the simulated topography. Simulated topographies obtained with a 3 μm fwhm Gaussian beam (a,b) for a translation mean path $L = 100$ nm after 2000 and 3000 iterations, respectively, and (c) for a translation mean free path $L = 150$ nm after 2000 iterations. Topographies are similar when the product of L by the number of iterations is conserved.

Finally, Figure 6 shows the tracking of two molecules in an electromagnetic gradient, illustrating the multiscale aspect of our model. The field gradient extent is typical of an interferometric pattern for SRG generation (2 μm pitch). In Figure 6b,c, the total displacement of the molecules and the field intensity for each position occupied by the molecules during the migration are plotted. As expected, molecules in the intense region easily move until they reach the low intensity region. It is also worth noting that this situation takes place after a subtle transient regime. For example, due to its initial orientation (toward the bright zone), molecule 2 travels to a brighter region before escaping from this region to a darker region. This subtle mechanism is believed to be the fundamental mechanism leading to the experimentally observed mass transport in azobenzene-containing films.

Relying on this multiscale aspect of our simulation, it appears that molecules do not simply migrate from high to low intensity regions. The matter accumulation is related to a statistical trapping effect where molecules in low intensity regions are less mobile than in other high intensity regions. The molecule can thus also migrate from low to high intensity even though these events have a lower probability.

The very good agreement between our calculations and experimental results on a wide length-scale validates the fundamental hypotheses of our photoinduced molecular diffusion model. Particularly, the motion of the photoactivated molecules could be compared to the diffusion mechanism occurring for molecules in a polymer matrix as expected in the free volume theory.

CONCUSIONS

In conclusion, Monte Carlo calculations based on our photoinduced molecular diffusion model that incorporates fundamental molecular dipole interactions with an illumination field can accurately predict molecular transport and topography modifications in photoisomerizable azobenzene-containing polymer films. The model incorporates long- and short-range molecular interactions, as well as assumptions regarding operation near T_g for optimized molecular motion. Ultimately, the model is robust and works for a wide range of illumination conditions, including both far-field and near-field illumination involving complex polarization states. Particularly, we have shown the versatility of our model by the calculation of the topography obtained on a plasmonic "bow-tie" antennae. Furthermore, the path of single molecules can be accurately described, and molecular photo-orientation can be predicted. Our model and experimental approach will be of use for imaging and lithography in the micro- and nanoscale regime and for developing new optical molecular nanomotors based on the use of complex plasmonic near-fields.

METHODS

Theoretical Calculations. We work with a 3D grid of molecular position space. Dipole vectors representing the dye molecules are distributed randomly within the polymer region consistent with typical experimental densities (0.2−0.3 grafting density). We allow for 54 discrete dipole orientations, as shown Figure 7a. A small, continuous random variation of the molecular orientation (Figure 7b) is taken in the evaluation of the absorption probability with each iteration in order to smooth the effects of discretization. The reorientation is randomly determined by considering the adjacent orientations relative to the actual orientation of the molecule, as shown Figure 7c.

To refine the photoinduced molecular motion, additional effects are then taken into account to move a dye molecule. Related to the three fundamental hypotheses, a molecule must absorb a photon to undergo a trans−cis−trans cycle and will move along its dipole axis according to the joint probability $P_{A\rightarrow B}$. Yet, when the destination density is not favorable, the movement direction can be slightly changed to account for the modification induced by the environment on the molecular trajectory. This effect allows one to take into account energy minimization considerations on the molecular trajectory. Moreover, local relaxation is dynamically addressed after each molecular movement by monitoring the surrounding molecules. Indeed, the vacancy left by the molecule can induce a strong discontinuity in the local density; surrounding molecules are then slightly moved to ensure the continuity of the density. The convergence of the simulated topography is then obtained when no favorable destinations (density wise) are accessible for the molecule undergoing trans−cis−trans isomerization. At this point, the other molecules are unlikely to undergo isomerization because of either their orientation or localization related to the local field intensity. Convergence is typically reached after a few thousand iterations, depending on the complexity of the local electromagnetic field.

Regarding the photoinduced translation length L, the average length is a consequence of the 54 orientational discretizations (Figure 7a). Defined relative to the second neighbors, these vectors account for the orientation of the molecule and the translation vector consecutive to an isomerization. The average value of L thus has a length that extends through two boxes. However, depending on the discretization cell, L takes on very different values. In the case of far-field experiments, for a 2 μm fwhm (full width at half-maximum) Gaussian beam and a grid of 100 × 100 boxes, $L \approx 40$ nm. For nanoscale studies, the value of L is much smaller ($L \approx 2$ nm). Yet, this variability of the translation length has no impact on the migration mechanisms as previously suggested for the anisotropic diffusion model.[13] In the particular context of our model, this impact is examined in Figure 8.

The mass migration has been simulated using a 3 μm fwhm Gaussian beam for a 50 nm (Figure 8a,b) and a 75 nm cell (Figure 8c). The respective values of L are, in these cases, $L = 100$ and 150 nm. The simulated topographies have similar features, yet the calculation time necessary to obtain the topography with $L = 100$ nm is larger. Indeed, if the size of the illumination field is the same, the mass migration is slower for small values of L. A larger number of molecular migration steps is necessary to cover a given length in comparison to the migration for higher values of L. This impact of the translation mean path, L, on the migration dynamics also appears in the anisotropic migration model where the photoinduced flux is constant when the product of L and α is constant (where α is the elementary diffusion rate).[13] This point is underlined in Figure 8, where a similar topography is obtained for $L = 100$ and 150 nm after 3000 and 2000 iterations, respectively. Since the diffusion rate is unchanged in our simulation, the same topography can be achieved if the product of L with the number of iterations is conserved while changing the value of L. In our calculation, the choice of L is made depending on the area of the zone simulated and the grid size. To maintain computation time reasonably small, the grid size is generally of 100 × 100 or 200 × 200 depending on the level of detail desired.

Acknowledgment. The authors are grateful to C. Hubert for providing us experimental materials for Figure 4. One of the author's PhD research (M.J.) is supported by the European Social Fund and the Conseil Général de l'Aube (distric grant). This work was financially supported by the ANR (2007 "photohybrid") and the Région Champagne-Ardennes (projet emergence E2007-08052). Use of the Center for Nanoscale Materials and work at Argonne National Laboratory were supported by the U.S. Department of Energy, Office of Science, Office of Basic Energy Science, under Contract No. DE-AC02-06CH11357.

REFERENCES AND NOTES

1. Natansohn, A.; Rochon, P. Photoinduced Motions in Azo-Containing Polymers. *Chem. Rev.* **2002**, *102*, 4139–4175.
2. Cojocariu, C.; Rochon, P. Light-Induced Motions in Azobenzene-Containing Polymers. *Pure Appl. Chem.* **2004**, *76*, 1479–1497.
3. Gilbert, Y.; Bachelot, R.; Royer, P.; Bouhelier, A.; Wiederrecht, G.; Novotny, L. Longitudinal Anisotropy of the Photoinduced Molecular Migration in Azobenzene Polymer Films. *Opt. Lett.* **2006**, *31*, 613–615.
4. Hubert, C.; Rumyantseva, A.; Lerondel, G.; Grand, J.; Kotscheev, S.; Billot, L.; Vial, A.; Bachelot, R.; Royer, P.; Chang, S.; Gray, S. K.; Wiederrecht, G. P.; Schatz, G. C. Near-Field Photochemical Imaging of Noble Metal Nanostructures. *Nano Lett.* **2005**, *5*, 615–619.
5. Lagugné Labarthet, F.; Bruneel, J.-L.; Buffeteau, T.; Sourisseau, C.; Huber, M. R.; Zilker, S. J.; Bieringer, T. Photoinduced Orientations of Azobenzene Chromophores in Two Distinct Holographic Diffraction Gratings as Studied by Polarized Raman Confocal Microspectrometry. *Phys. Chem. Chem. Phys.* **2000**, *2*, 5154–5167.
6. Barrett, C.; Natansohn, A. L.; Rochon, P. L. Mechanism of Optically Inscribed High-Efficiency Diffraction Gratings in Azo Polymer Films. *J. Phys. Chem.* **1996**, *100*, 8836–8842.
7. Viswanathan, N. L.; Kim, D. Y.; Bian, S.; Williams, J.; Liu, W.; Li, L.; Samuelson, L.; Kumar, J.; Tripathy, S. K. Surface Relief Structures on Azo Polymer Films. *J. Mater. Chem.* **1999**, *9*, 1941–1955.
8. Viswanathan, N. L.; Balasubramanian, S.; Li, L.; Tripathy, S. K.; Kumar, J. A Detailed Investigation of the Polarization-Dependent Surface-Relief-Grating Formation Process on Azo Polymer Films. *Jpn. J. Appl. Phys.* **1999**, *39*, 5928–5937.
9. Pedersen, T. G.; Johansen, P. M. Mean-Field Theory of Photoinduced Molecular Reorientation in Azobenzene Liquid Crystalline Side-Chain Polymers. *Phys. Rev. Lett.* **1997**, *79*, 2470–2473.
10. Barada, D.; Itoh, M.; Yatagai, T. Numerical Analysis of Photoinduced Surface Relief Grating Formation by Particle Method. *J. Appl. Phys.* **2004**, *96*, 4204–4210.
11. Barada, D.; Fukuda, T.; Itoh, M.; Yatagai, T. Numerical Analysis of Photoinduced Surface Relief Grating Formation by Particle Method. *Opt. Rev.* **2005**, *12*, 271–273.
12. Barada, D.; Fukuda, T.; Itoh, M.; Yatagai, T. Photoinduced Chirality in an Azobenzene Amorphous Copolymer Bearing Large Birefringent Moiety. *Jpn. J. Appl. Phys.* **2006**, *45*, 6730–6736.
13. Lefin, P.; Fiorini, C.; Nunzi, J. Anisotropy of the Photo-Induced Translation Diffusion of Azobenzene Dyes in Polymer Matrices. *Pure Appl. Opt.* **1998**, *7*, 71–82.
14. Todorov, T.; Nikolova, L.; Tomova, N. Polarization Holography. 2: Polarization Holography Gratings in Photoanisotropic Materials with and without Intrinsic Birefringence. *Appl. Opt.* **1984**, *23*, 4588–4591.
15. Bellini, B.; Ackermann, J.; Klein, H.; Graves, C.; Dumas, P.; Safarov, V. Light-Induced Molecular Motion of Azobenzene-Containing Molecules: A Random-Walk Model. *J. Phys.: Condens. Matter* **2006**, *18*, S1817–S1835.
16. Bian, S.; Li, L.; Kumar, J.; Kim, D. Y.; Williams, J.; Tripathy, S. K. Single Laser Beam-Induced Surface Deformation on Azobenzene Polymer Films. *Appl. Phys. Lett.* **1998**, *73*, 1817–1819.
17. Kim, D. Y.; Tripathy, S. K.; Li, L.; Kumar, J. Laser-Induced Holographic Surface Relief Gratings on Nonlinear Optical Polymer Films. *Appl. Phys. Lett.* **1995**, *66*, 1166.

18. Rochon, P.; Batalla, E.; Natansohn, A. Optically Induced Surface Gratings on Azoaromatic Polymer Films. *Appl. Phys. Lett.* **1995**, *66*, 136.
19. Juan, M.; Plain, J.; Bachelot, R.; Royer, P.; Gray, S. K.; Wiederrecht, G. P. Stochastic Model for Photoinduced Surface Relief Grating Formation through Molecular Transport in Polymer Films. *Appl. Phys. Lett.* **2008**, *93*, 153304.
20. Fiorini, C.; Charra, F.; Nunzi, J.-M.; Raimond, P. Quasi-Permanent All-Optical Encoding of Noncentrosymmetry in Azo-Dye Polymers. *J. Opt. Soc. Am. B* **1997**, *14*, 1984–2003.
21. Delaire, J. A.; Nakatani, K. Linear and Nonlinear Optical Properties of Photochromic Molecules and Materials. *Chem. Rev.* **2000**, *100*, 1817–1846.
22. Lagugné-Labarthet, F.; Bruneel, J. L.; Rodriguez, V.; Sourisseau, C. Chromophore Orientations in Surface Relief Gratings with Second-Order Nonlinearity as Studied by Confocal Polarized Raman Microspectrometry. *J. Phys. Chem. B* **2004**, *108*, 6949–6960.
23. Hubert, C.; Bachelot, R.; Plain, J.; Kotscheev, S.; Lerondel, G.; Juan, M.; Royer, P.; Zou, S.; Schatz, G. C.; Wiederrecht, G. P.; Gray, S. K. Near-Field Polarization Effects in Molecular-Motion-Induced Photochemical Imaging. *J. Phys. Chem. C* **2008**, *112*, 4111–4116.